



Delft University of Technology

## Assessment of Noise Variability of Landing Aircraft Using Phased Microphone Array

Snellen, Mirjam; Merino Martinez, Roberto; Simons, Dick

**DOI**

[10.2514/1.C033950](https://doi.org/10.2514/1.C033950)

**Publication date**

2017

**Document Version**

Accepted author manuscript

**Published in**

Journal of Aircraft: devoted to aeronautical science and technology

**Citation (APA)**

Snellen, M., Merino Martinez, R., & Simons, D. (2017). Assessment of Noise Variability of Landing Aircraft Using Phased Microphone Array. *Journal of Aircraft: devoted to aeronautical science and technology*, 54(6), 2173-2183. DOI: 10.2514/1.C033950

**Important note**

To cite this publication, please use the final published version (if applicable).

Please check the document version above.

**Copyright**

Other than for strictly personal use, it is not permitted to download, forward or distribute the text or part of it, without the consent of the author(s) and/or copyright holder(s), unless the work is under an open content license such as Creative Commons.

**Takedown policy**

Please contact us and provide details if you believe this document breaches copyrights.

We will remove access to the work immediately and investigate your claim.

# Assessment of the noise variability of landing aircraft using a phased microphone array

Mirjam Snellen<sup>a</sup>, Roberto Merino-Martínez<sup>b</sup> and Dick G. Simons<sup>c</sup>

*Delft University of Technology, 2629 HS Delft, the Netherlands*

Enforcing noise control environmental laws around airports is a difficult task due to the large variability in the noise levels observed for flyovers of the same aircraft type under similar conditions. These variations are not properly considered by the current models, such as the Noise-Power-Distance tables. In this research, noise measurements of aircraft flyovers are used to assess this variability and investigate its causes. 115 flyovers of landing aircraft were recorded using a 32 microphone phased array. It was assumed that the main cause of this variability is the change of the emitted aircraft noise, as previous studies showed that the effect of the variable atmosphere (for the distances considered) is negligible. The noise level variability for the Boeing 737 and Fokker 70 cases was approximately 7 dB. The fan rotational speed of each flyover was determined by analyzing the spectrograms. Functional beamforming was applied to the acoustic data. For the Boeing 737 case it was found that the engines are the dominant noise source for all flyovers and that over 75% of the variation of the noise levels can be explained by variations in the engine settings. The Fokker 70 flyovers were dominated by airframe noise sources. Differences in the aircraft velocity explain almost 70% of the noise level variability in this case.

<sup>a</sup> Associate professor, Aircraft Noise & Climate Effects section, Faculty of Aerospace Engineering, Kluyverweg 1.

<sup>b</sup> PhD candidate, Aircraft Noise & Climate Effects section, Faculty of Aerospace Engineering, Kluyverweg 1. AIAA

Student Member. E-mail: r.merinomartinez@tudelft.nl

<sup>c</sup> Full professor, Aircraft Noise & Climate Effects section, Faculty of Aerospace Engineering, Kluyverweg 1.

## I. Introduction

Aircraft noise is one of the major current issues to be dealt with by the aerospace industry. Apart from being annoying, noise pollution can even lead to severe health problems, such as hypertension, sleep deprivation and harmful cognitive effects [1]. Even though individual aircraft have experienced large noise reductions over the last decades, the continuous growth of air traffic (around 5% per year [2]) is expected to aggravate the problem even more in the future.

This issue is dealt with through strict noise regulations and night curfews which consequently limit airport capacity. To assess noise exposure, most airports use models which employ the so-called Noise-Power-Distance (NPD) tables, such as the Integrated Noise Model (INM) [3–7]. These tables contain Sound Pressure Level (SPL or  $L_p$  data) for different aircraft types and for predefined distances and power settings depending on the flight procedure (since the actual power settings are typically unknown). Thus, these models provide a unique noise level value for a certain aircraft type flying in a certain flight phase and at a certain distance. Measurements showed  $L_{p,A}$  variations as large as 12 dB for the same aircraft type [8], flight procedure and location. This variability is assumed to be caused mostly due to the combined effects of the changing atmospheric conditions and the variations of the emitted noise at the source. Other studies [9, 10] showed that the variability contribution due to the changing atmosphere is typically less than 2 dB for distances up to 100 m, as considered in this paper. Therefore, this research will assume that the variability due to the noise source (i.e., the aircraft) is dominant [10].

The aim of this research is to investigate the causes for the variability of the noise levels emitted by the aircraft. Use was made of noise measurements taken for 115 flyovers at Amsterdam Airport Schiphol using a 32 microphone phased array. The aircraft were flying in operational conditions, i.e., their operation was not adapted for this research in any way. Benefits are that the measurements are fully representative of the actual situation. However, unknowns, such as the engine settings and aircraft trajectories need to be determined with care. The measurements taken correspond to landing aircraft, which typically have more regular trajectories than during takeoff. The use of a microphone array allows for the application of beamforming algorithms to the acoustic data, which provide source plots, also known as acoustic images, depicting the location and  $L_p$  of the sound

sources on the aircraft. Moreover, the effects of background noise and ground reflection are largely reduced [10]. For this research, use was made of functional beamforming [11, 12]. This method has a better array resolution (i.e., the beam width of the main lobe 3 dB under its peak [13]) than conventional beamforming, which is highly beneficial for the flyover measurements considered in this paper, due to the large distance between source and observer. This way, the noise emissions of single elements from the aircraft can be separated and studied in terms of frequency.

This research is a continuation of the work done by Simons et al. [10] in which the variations in the noise levels for a limited number (fewer than ten) of Boeing 737 flyovers at Rotterdam The Hague Airport were studied. The current paper expands this research investigating more aircraft types. In addition, functional beamforming is applied. This provides highly detailed source plots, allowing a good discrimination of the different aircraft noise sources. From these source plots, a distinction can be made between the noise from the engines and the airframe. Therefore, in this research airframe noise is also considered and studied in terms of variability.

Section II summarizes the experimental setup of the presented research and the aircraft trajectory estimation methods used. The beamforming method employed in this research is briefly explained in Sec. III. An explanation on how to derive the engine fan settings of an aircraft from the acoustic data can be found in Sec. IV. Section V presents the results from the analysis of the flyover measurements, and finally Sec. VI contains the conclusions.

## II. Experimental setup

A total of 115 flyover measurements were recorded at Amsterdam Airport Schiphol using a 32 microphone phased array in a spiral distribution [14, 15]. The array diameter was 1.7 m and the data were band filtered in the frequency range from 45 Hz to 11,200 Hz. The sampling frequency employed was 40 kHz. Moreover, an optical camera was integrated into the center of the array at a fixed angle facing straight up from the ground. The microphone array was located 1240 m to the south of the threshold of the Aalsmeerbaan runway (36R), mainly used for landing. More information about the experimental setup and the array response characteristics can be found in [14]. The aircraft positions will be referred to the distances relative to the array, with the Y axis in the direction of the runway (with decreasing values for approach) and the X axis perpendicular to

Table 1: Meteorological conditions at Amsterdam Airport Schiphol at 12:00 A.M. [16].

Variable	June 18 <sup>th</sup> 2013	August 8 <sup>th</sup> 2013
Temperature	27.2°C	20.3°C
Humidity	56 %	61 %
Air pressure	101,500 Pa	101,890 Pa
Precipitation	0 mm	0 mm
Wind speed (at 10 m height)	2 m/s	5 m/s
Wind direction (at 10 m height)	160°	340°

it.

Measurements were taken on two different days. Table 1 contains the most relevant meteorological data for those days at 12:00 A.M., as provided by the Royal Netherlands Meteorological Institute, KNMI [16]. The values for the same parameters are available every hour. The sound speed,  $c$ , and the atmospheric absorption coefficient,  $\alpha$ , depend on these meteorological conditions and, therefore, require to have their variations taken into account.

The measurements taken correspond to 13 different aircraft families depending on their engine [17], see Table 2. The Boeing 737 “Next Generation” (700, 800 and 900 series) is the most frequently occurring, with 50 flyover measurements available. This set of series was considered as a collective since they have the same engine, wing area, wing span and nose landing gear geometries, which are the objects of study in this paper.

The aircraft trajectories need to be accurately known to properly take into account the propagation, moving source and Doppler effects, as will be explained in Sec. III A. Three different approaches were employed to calculate the aircraft position and velocity [14]: the ADS-B (Automatic Dependent Surveillance-Broadcast), the ground radar from air traffic control and the extrapolation of the optical camera images. All three methods provided similar results (with variations up to 6%). The extrapolation of the optical camera images was used mainly because of its ease to overlay the beamforming results on to the optical frames. The average flight height and average aircraft velocity overhead were 67 m and 271 km/h, respectively. Henceforth, true air speeds (considering the wind

Table 2: Aircraft types with their correspondent engine [17] and the number of recorded measurements for each type. Here  $n_{max}$  corresponds to the maximum fan rotational speed (at 100% engine fan settings) in rpm [17].

Aircraft type	Amount	Engine type	No. of fan blades, $B$	$n_{max}$ [rpm]
Airbus 300	1	CF6-80C2A5	38	3320
Airbus 320 (CFM)	4	CFM56-5B5/P	36	5000
Airbus 320 (IAE)	3	IAE V2500-A1	22	5465
Airbus 380	1	GP7270	24	2467
Boeing 737 (series 300, 400 and 500)	9	CFM56-3C1	38	5175
Boeing 737 (series 700, 800 and 900)	50	CFM56-7B	24	5175
Boeing 747	4	CF6-80C2B1F	38	3280
Boeing 767	1	PW 4060	38	3600
Boeing 777	6	GE90-94B	22	2262
Embraer 145	1	RR AE3007A1	24	8700
Embraer 190	11	GE CF34-10E5	24	5954
Fokker 70	23	RR TAY 620	22	8100
McDonnell Douglas 81	1	PW JT8D-217C	24	8219

speeds) are presented in this paper.

### III. Beamforming methods applied

#### A. Description of the preprocessing of the acoustic data

For the case of flyover measurements, several corrections need to be applied to the acoustic data before performing any further analysis or applying beamforming.

First of all, the background noise needs to be taken into account, such as the noise generated by the microphone array electronics and the ambient noise. Therefore, all the  $L_p$  values in the spectrograms under a threshold value of 30 dB (typical  $L_p$  in a quiet library) were neglected, to avoid amplification errors later on.

Afterwards, the Doppler effect due to the relative motion of the aircraft with respect to the observer needs to be considered. The expression for the Doppler shifted frequency,  $f'$ , is

$$\frac{f'}{f} = \frac{1}{1 - \|\mathbf{M}\| \cos(\theta)} \quad (1)$$

This equation determines the frequency shift due to the Doppler effect, where  $f'$  is the observed frequency,  $f$  is the emitted frequency,  $\mathbf{M}$  is the Mach number vector,  $\mathbf{M} = (M_x, M_y, M_z) = \left( \frac{V_x}{c}, \frac{V_y}{c}, \frac{V_z}{c} \right) = \frac{\mathbf{V}}{c}$ ,  $\mathbf{V}$  is the source velocity vector,  $c$  is the speed of sound, and  $\theta$  is the angle between the relative position vector of the source with respect to the observer,  $\mathbf{r}$ , and the source velocity vector,  $\mathbf{V}$ . The last two parameters are known from the aircraft trajectory estimation explained in Sec. II. The Doppler effect can be observed in the varying frequency of the engine tones in the spectrogram, see Fig. 1 (a). This phenomenon is corrected by resampling the acoustic data according to Howell et al. [18].

Lastly, the propagation effects have to be accounted for, to obtain the actual  $L_p$  values at the source [19, 20]. The  $L_p$  at the source position, namely at a distance of one meter ( $r_0 = 1$  m), is estimated by adding the transmission losses due to the geometrical spreading and the atmospheric absorption to the sound recorded at the observer position at a distance  $r$  as

$$L_p(r_0, f) = L_p(r, f) + 20 \log \left( \frac{r}{r_0} \right) + \alpha(f) r \quad (2)$$

The atmospheric absorption coefficient,  $\alpha$ , depends on the sound frequency, and the temperature, relative humidity and static pressure of the atmosphere [19, 20].

The result of all the aforementioned corrections is depicted in Fig. 1 in the form of two spectrograms: the picture on the left represents the spectrogram at the array before any correction and the picture on the right the spectrogram at the source after correcting the data. Notice the different decibel color scales and the change in the Doppler shifted tones to straight lines.

## B. Functional beamforming

Functional beamforming is a beamforming technique developed by Dougherty [11, 12]. This method is based on the conventional frequency domain beamforming algorithm (CFDBF) [21, 22], also known as delay-and-sum, which is the most widely used method for aeroacoustic experiments

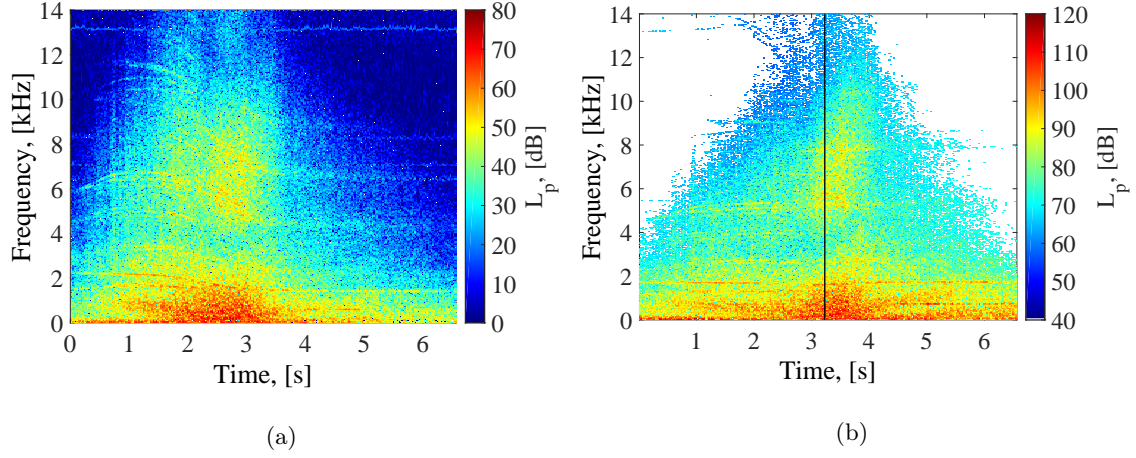


Fig. 1: (a) Spectrogram recorded at the array during an Airbus A321 flyover. (b) Spectrogram at the source position ( $r_0 = 1$  m) after applying the propagation and source motion corrections. The white part represents the background noise deletion and the solid black line represents the time overhead.

[23–31]. Functional beamforming depends on an exponent parameter,  $\nu$ , which needs to be set by the user. The formulae for the general case of an  $N$ -microphone array are described below.

Firstly, the cross-spectral matrix ( $\mathbf{C}$ ) is expressed as its eigenvalue decomposition:

$$\mathbf{C} = \frac{1}{2} \mathbf{p} \mathbf{p}^* = \mathbf{U} \boldsymbol{\Sigma} \mathbf{U}^* \quad (3)$$

where an asterisk,  $(\cdot)^*$ , denotes the complex conjugate transpose,  $\mathbf{p} = \mathbf{p}(f) \in \mathbb{C}^{N \times 1}$  contains the Fourier transform of the recorded Doppler-shifted pressure amplitudes for each microphone at a frequency  $f$ ,  $\mathbf{U}$  is a unitary matrix whose columns are the eigenvectors  $(\mathbf{u}_1, \dots, \mathbf{u}_N)$  of  $\mathbf{C}$  and  $\boldsymbol{\Sigma}$  is a diagonal matrix whose diagonal elements are the eigenvalues  $(\sigma_1, \dots, \sigma_N)$  of  $\mathbf{C}$ .

For beamforming, a scan grid is defined containing all the potential sound source positions. For each grid point, a steering vector,  $\mathbf{g}_j \in \mathbb{C}^{N \times 1}$ , is determined, which accounts for the phase shifts and change in amplitude between the source and the microphones. For a general grid point with position vector  $\boldsymbol{\xi}_j$ , the steering vector has  $N$  components,  $g_{j,n}$ ,  $n = 1 \dots N$ , which are the modeled pressures at each microphone location for a source at that grid point with unit strength [32]:

$$g_{j,n} = \frac{-\exp(-2\pi i f \Delta t_{j,n})}{4\pi \|\boldsymbol{x}_n - \boldsymbol{\xi}_j\| (1 - \|\boldsymbol{M}\| \cos \theta)^2} \quad (4)$$

where  $\|\cdot\|$  denotes the Euclidean norm of a vector,  $i = \sqrt{-1}$ ,  $\Delta t_{j,n}$  is the time delay between the emission and the reception of the signal by the observer (i.e., from the grid point to the microphone) and  $\boldsymbol{x}_n = (x_n, y_n, z_n) \in \mathbb{R}^{N \times 3}$ ,  $n = 1 \dots N$ , are the position vectors of the  $N$  microphones. In the case of a moving sound source, like an aircraft flying by,  $\boldsymbol{M} \neq \mathbf{0}$  and the term in parentheses in the denominator in Eq. 4 represents the so-called convective amplification [19]. The moving source effect also needs to be taken into account for calculating the time delay [14, 18, 23],  $\Delta t_{j,n}$ :

$$\Delta t_{j,n} = \frac{-\boldsymbol{M} \cdot (\boldsymbol{x}_n - \boldsymbol{\xi}_j) + \sqrt{(\boldsymbol{M} \cdot (\boldsymbol{x}_n - \boldsymbol{\xi}_j))^2 + \beta^2 \|\boldsymbol{x}_n - \boldsymbol{\xi}_j\|^2}}{c\beta^2} \quad (5)$$

where  $\beta$  is a parameter defined as

$$\beta = \sqrt{1 - \|\boldsymbol{M}\|^2} \quad (6)$$

The expression for the functional beamformer for a grid point located at  $\boldsymbol{\xi}_j$  and an exponent value of  $\nu$  is

$$A_\nu(\boldsymbol{\xi}_j) = \left[ \boldsymbol{w}_j^* \boldsymbol{C}^{\frac{1}{\nu}} \boldsymbol{w}_j \right]^\nu = \left[ \boldsymbol{w}_j^* \boldsymbol{U} \boldsymbol{\Sigma}^{\frac{1}{\nu}} \boldsymbol{U}^* \boldsymbol{w}_j \right]^\nu \quad (7)$$

Here  $A_\nu$  is the estimate for the source autopower at the grid point  $\boldsymbol{\xi}_j$ . Notice that the case with  $\nu = 1$  corresponds to the CFDBF formula. In Eq. 7,  $\boldsymbol{w}_j \in \mathbb{C}^{N \times 1}$  is the normalized steering vector,  $\boldsymbol{g}_j$ , for that grid point  $\boldsymbol{\xi}_j$ . Different steering vector normalizations are found in the literature [33], but none of them is able to provide the exact source location and the correct source strength at the same time, although the errors are typically small for acoustic sources close to the zenith, as considered here. In this research, two different normalizations were employed. The first one provides the correct source position (Eq. 8) and the second one, the correct source strength (Eq. 9).

$$\boldsymbol{w}_{j_{pos}} = \frac{\boldsymbol{g}_j}{\|\boldsymbol{g}_j\|} \quad (8)$$

$$\mathbf{w}_{j_{str}} = \frac{\mathbf{g}_j}{\|\mathbf{g}_j\|^2} \quad (9)$$

An approximate solution is to first determine the source plot with the correct source positions substituting Eq. 8 in Eq. 7 and later correct the sound pressure levels of the whole source map according to the ones obtained when using Eq. 9 in Eq. 7. In this way, a satisfactory combination of estimating both source strength and location is achieved.

The performance of the functional beamforming algorithm depends on the value of the exponent  $\nu$ . This can be seen when considering a single sound source of amplitude  $s_k$  at position vector  $\xi_k$ . In that case, the dominant eigenvalue of  $\mathbf{C}$  will be  $\sigma_1 = s_k^2/2$  with the corresponding eigenvector  $\mathbf{u}_1 = \mathbf{g}_k$ . Using Eqs. 7 and 9, the functional beamforming autopower value for a general location  $\xi_m$  with steering vector  $\mathbf{g}_m$ , i.e., the Point Spread Function (PSF), will now be:

$$A_\nu(\xi_m) = [\mathbf{w}_{m_{str}}^* \mathbf{C}^{\frac{1}{\nu}} \mathbf{w}_{m_{str}}]^\nu = \left[ \frac{\mathbf{g}_m^* \left( \frac{s_k^2}{2} \mathbf{g}_k \mathbf{g}_k^* \right)^{\frac{1}{\nu}} \mathbf{g}_m}{\|\mathbf{g}_m\|^4} \right]^\nu = \frac{s_k^2}{2} \left[ \frac{\mathbf{g}_m^* \mathbf{g}_k \mathbf{g}_k^* \mathbf{g}_m}{\|\mathbf{g}_m\|^4} \right]^\nu = \frac{s_k^2}{2} \left[ \frac{(\mathbf{g}_m^* \mathbf{g}_k)^2}{\|\mathbf{g}_m\|^4} \right]^\nu \quad (10)$$

It can be observed that the factor multiplying the source strength is powered to the exponent  $\nu$ . This factor has a value of one at the correct source locations and alias points (i.e., the so-called grating lobes) and smaller than one everywhere else. Therefore, powering this factor at a sidelobe with an exponent larger than 1 will lower its level, leaving the true sources  $L_p$  values identical if an appropriate grid is used. The advantage of functional beamforming is that it preserves lower amplitude noise sources, in contrast with just powering the CFDBF source map by a factor  $\nu$ . For ideal conditions, the dynamic range (in decibels) for the functional beamforming increases linearly with the exponent value,  $\nu$ . Thus, for an appropriate exponent value the dynamic range is significantly increased. The main lobes will also be sharpened, improving the array spatial resolution to some extent. However, the minimum distance at which two coherent sources can be separated as two different sources is still limited by the Rayleigh criterion [14, 34]. The computational time for the functional beamforming is practically identical to the CFDBF one, because the only relevant additional operation is the eigenvalue decomposition of  $\mathbf{C}$ , which is typically faster than the rest of

the steps involved in the beamforming process.

In previous work functional beamforming has been applied to numerical simulations [11, 12, 14], idealized cases with speakers as experimental noise sources and controlled experiments with components in a laboratory [11, 12]. This algorithm was also tested very recently [14, 35–37] on full-scale aircraft during operational conditions indicating a dynamic range approximately 30 times larger and an array spatial resolution 6 times better than the CFDBF. These qualities make functional beamforming a suitable method for flyover measurements.

#### IV. Determination of the engine fan settings

Fan noise is usually a dominant noise source for turbofan aircraft during landing, especially in the forward direction [19, 38]. It is mainly generated by the interaction between the fan blades and the stator vanes and it often presents a strong tonal sound component. Differences in the fan rotational speed are expected to be measured for the same aircraft type [10], since this variable depends on several conditions, such as the aircraft mass, wind situation or flap settings.

The fan fundamental frequency,  $f_1$ , is also known as the Blade Passing Frequency (BPF) and it can be calculated using:

$$\text{BPF} = f_1 = \frac{B n}{60} \quad (11)$$

where  $B$  is the number of blades of the fan (see Table 2) and  $n$  is the fan rotational speed measured in rpm.

It is common to find the presence of higher harmonics of the BPF in the frequency spectra as well. The frequencies of these harmonics,  $f_k$ , are the multiples of the BPF ( $f_1$ ):

$$f_k = k f_1, \quad k = 1, 2, 3 \dots \quad (12)$$

In order to work with specific variables, the fan rotational speed,  $n$ , is divided by the maximum fan rotational speed,  $n_{max}$ , to obtain the specific fan speed percentage, also known as  $N1\% = 100 n/n_{max}$  as it refers to the low pressure spool. Henceforth,  $N1\%$  will be referred to as the engine

fan setting and is considered to be constant during the measurement time, for simplicity. Even if pilots sometimes vary the engine settings in that interval, the agreement of the calculated engine settings with the measured ones was satisfactory for all flyovers, observing the spectrograms.

The first step of this analysis is to determine the fan BPF of each flyover using the spectrograms, to calculate the fan rotational speed with Eq. 11. For this study, the forward arc spectra, i.e., the sound when the aircraft is approaching the array, is employed. After extracting a time interval (from 1.5 to 1 s before the time overhead, corresponding to emission angles between  $\theta = 37^\circ$  to  $63^\circ$ , respectively) of the forward arc from the spectrogram (see Fig. 2 (a)), the Doppler-corrected spectra are averaged over time and a polynomial fit is applied to the averaged spectrum, representing the broadband noise as presented in Fig. 2 (b). This polynomial is then subtracted from the spectrum and the difference is squared to observe the engines tonal peaks in a better way (only positive differences are considered). This magnitude is called squared residual and it is used to calculate the BPF and its harmonics.

After selecting all the peaks of interest (higher than a threshold amplitude) from the squared residual vector, three different methods [39] are employed to determine the engine fan settings of each flyover:

1. Method 1 considers all the possible combinations of three peaks for all the selected peaks as candidates for being the BPF or its harmonics. It uses a least-squares regression to estimate a BPF value and its corresponding harmonics for each combination. The four values with the smallest deviation between the modeled and the measured peaks are selected as candidates for being harmonics of the BPF.
2. Method 2 uses the three considered peaks with lowest frequency and the differences between them as potential candidates for being the BPF. The selected BPF value is the one whose harmonics coincide with the largest number of peaks, as long as it provides a realistic value for  $N1\%$ .
3. Method 3 employs a synthetic noise model for the full expected spectrum. An iterative process is performed varying the engine fan settings  $N1\%$ , i.e., the BPF value, within a realistic range.

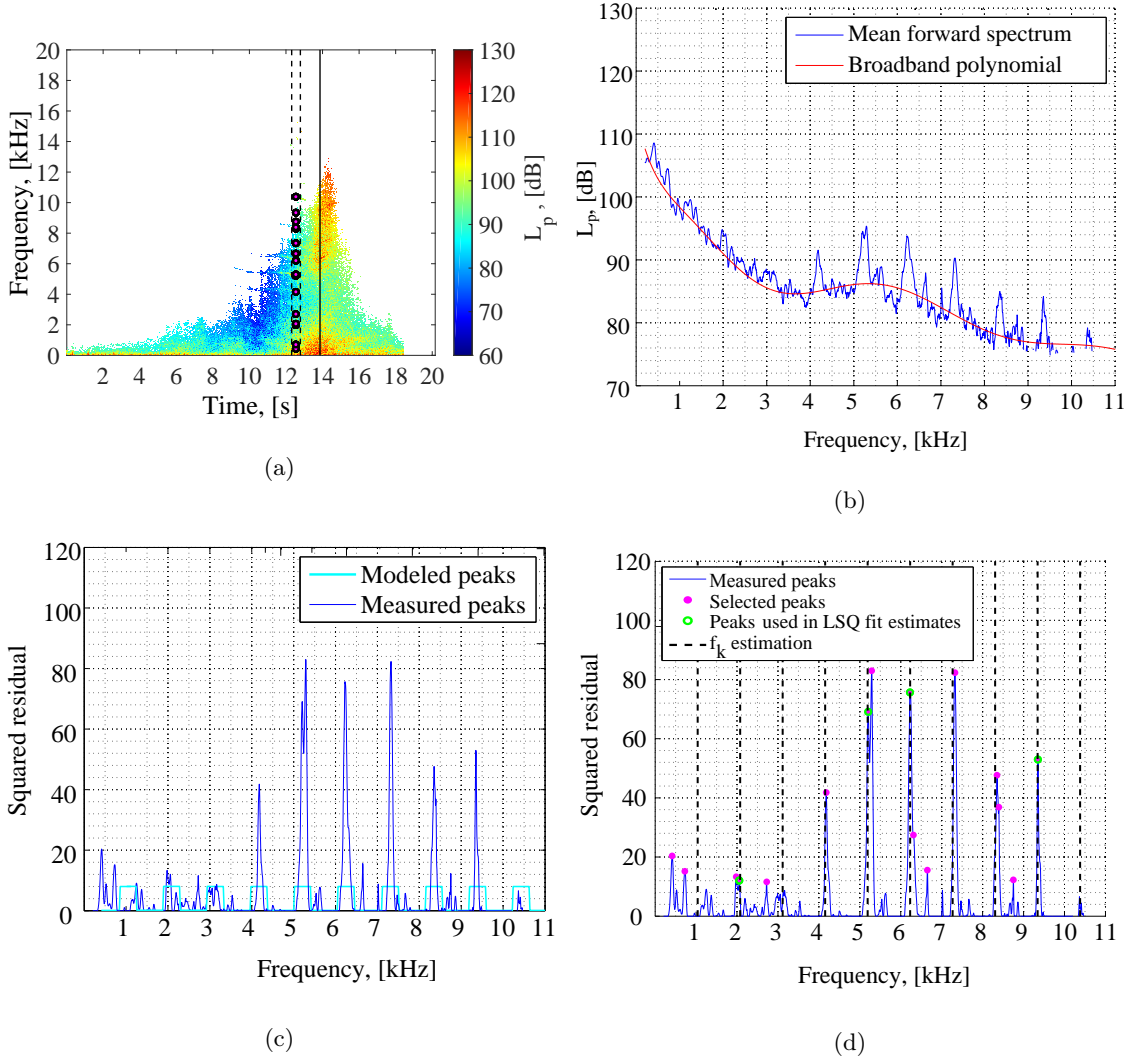


Fig. 2: (a) Spectrogram at the source of a Boeing 737-800 flyover. The solid black line represents the time overhead and the black dashed lines the selected time window. The circles show the peaks considered. (b) Mean forward spectrum and the 10<sup>th</sup> degree broadband polynomial fit. (c) Comparison between the modeled and measured peaks for method 3. (d) BPF estimation results for method 1.

The engine fan settings value resulting in the maximum correlation between the modeled and the experimental data is selected as the candidate, as shown in Fig. 2 (c).

Figure 3 explains the process for estimating the BPF value using the aforementioned methods. An example of the results obtained by the first method is depicted in Fig. 2 (d). The spectrograms need to be individually studied with great care and the outcomes of the three methods evaluated

depending on their agreement with the spectra. Even if the three methods normally provide similar results, it is required to confirm whether the solution has a realistic value and whether it explains as many harmonics as possible. In case the value obtained for  $N1\%$  is not realistic, a different time interval is chosen until this condition is met.

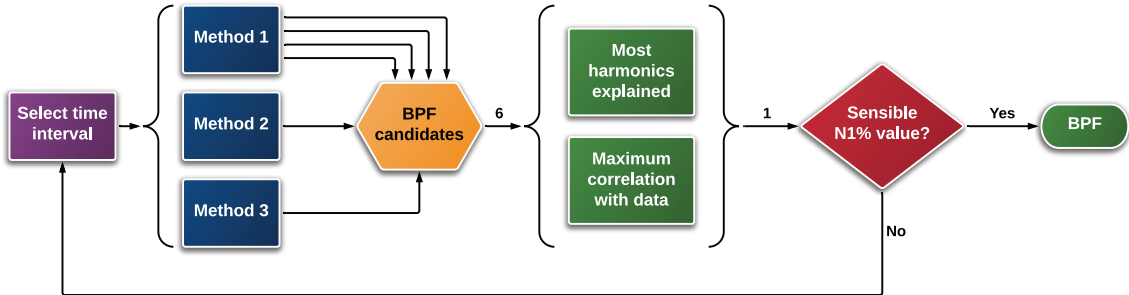


Fig. 3: Flowchart showing the process for estimating the BPF value using the three different methods.

The estimated engine fan settings ( $N1\%$ ) range in this research varies from 40% to 70%, which are typical values for commercial planes during the landing phase.

## V. Experimental results

### A. Assessment of overall $L_{p,A,max}$ and $L_{p,A,e}$ variations using a single microphone

The maximum overall  $L_{p,A}$  (also known as OASPL or  $L_{p,A,max}$ ) at the source location ( $r_0 = 1$  m) and the Sound Exposure Level ( $L_{p,A,e}$  or SEL) were calculated for each flyover. Both metrics are obtained from the spectrograms. The first one is calculated as the maximum overall  $L_{p,A}$  at the source. The second metric is determined by integrating the overall  $L_{p,A}$  time series at the array position between the two instants with an overall  $L_{p,A}$  10 dB<sub>A</sub> lower than the maximum [20].

The obtained results for both metrics are gathered in the boxplots in Fig. 4, where the aircraft types are presented at the  $x$ -axis in order of increasing size. It can be noticed that the Boeing 747 and Boeing 777 generate the highest noise metrics in both cases, as it could be expected, due to their considerably larger size. The differences between both boxplots values are due to the fact that the  $L_{p,A,e}$  considers the sound perceived at the array and the duration of the sound, but, in general, the tendencies between aircraft types are similar in both figures. Variations for the same aircraft

type as large as 7 dB for the  $L_{p,A,max}$  and 6 dB for the  $L_{p,A,e}$  can be observed.

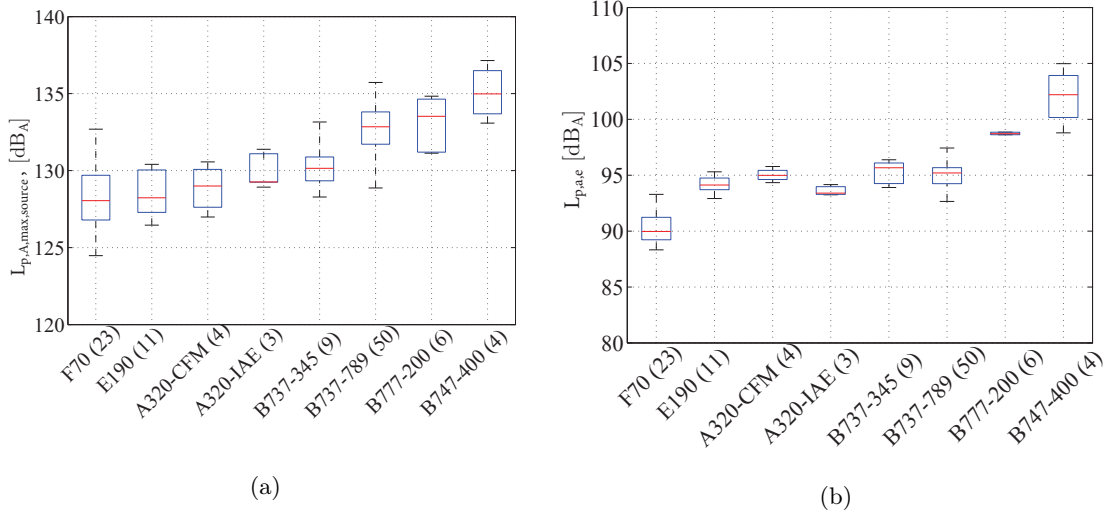


Fig. 4: Boxplot of the (a)  $L_{p,A,max}$  at the source position (b)  $L_{p,A,e}$  for the different aircraft types. On each box, the central mark is the median, the edges of the box are the 25<sup>th</sup> and 75<sup>th</sup> percentiles and the whiskers extend to the most extreme data points.

This variability is also present in the flyover sound frequency spectra and is even larger for single frequencies, as it can be seen in the examples depicted in Fig. 5 for the Boeing 737 (series 700, 800 and 900) and Fokker 70 cases. The frequency axis for each spectrum was normalized by the corresponding BPF obtained in Sec. IV. The time interval chosen for this spectral analysis was 1.5 to 1 s before the time overhead (forward arc). The relatively large contribution of the BPF harmonics can be observed in a clear way for the Boeing 737 “Next Generation” in Fig. 5 (a), where the peaks from the third to the eighth harmonic align in a satisfactory manner. On the other hand, the harmonic tones are not so distinguishable for the Fokker 70 case, see Fig. 5 (b). However, the fan tones were clearly detected in all cases.

As an attempt to explain these variations of the noise levels, a correlation study was performed with respect to the engine fan settings  $N1\%$  (calculated in Sec. IV) and the aircraft velocity, which was estimated as explained in Sec. II. As a first approach, the  $L_{p,A,max}$  at the source was used, without any beamforming method applied and without focusing on any specific frequency.

The results presented in Figs. 6 and 7 correspond to the Boeing 737 “Next Generation” and

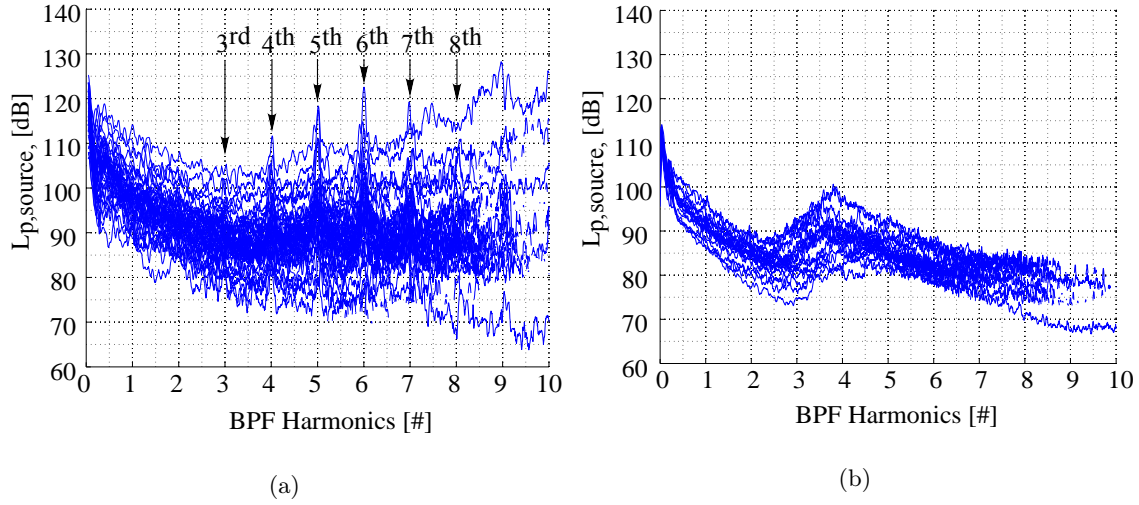


Fig. 5: Flyover spectra at the source position with the frequencies normalized with respect to the BPF harmonics for (a) the Boeing 737 (series 700, 800 and 900) and (b) Fokker 70. The time interval selected was from 1.5 s before the time overhead to 1 s before the time overhead.

the Fokker 70 cases because they are the two most numerous aircraft types in this research. The correlation coefficient,  $\rho$ , the coefficient of determination,  $\rho^2$ , and the  $p$ -value are calculated and depicted in each plot. The linear least-squares fit is also included. It can be observed that there is a significant correlation in all cases, especially with the engine fan settings. Also interesting is the relatively large correlation ( $\rho \approx 0.55$ ) found between the maximum overall  $L_{p,A}$  and the aircraft velocity for the Fokker 70 case.

The  $p$ -value is a measure of the significance of the correlation between two variables. It expresses the possibility to obtain that particular correlation coefficient in case the variables were uncorrelated. Thus, it should be as low as possible. In these eight examples the  $p$ -values are considerably lower than the typical threshold value of 0.05, meaning that all the correlations found are significant. The coefficient of determination,  $\rho^2$ , expresses the fraction of the variance in the two variables which is shared. For instance, for the Boeing 737 case, the  $L_{p,A,max}$  vs. the engine settings present  $\rho^2 \approx 0.45$ , i.e., almost 45% of the total variance observed in the  $L_{p,A,max}$  can be explained by the changes in the fan rotational speed, and 16% is explained by variations in the aircraft velocity. For the Fokker 70 these numbers amount to 37% and 30%, respectively.

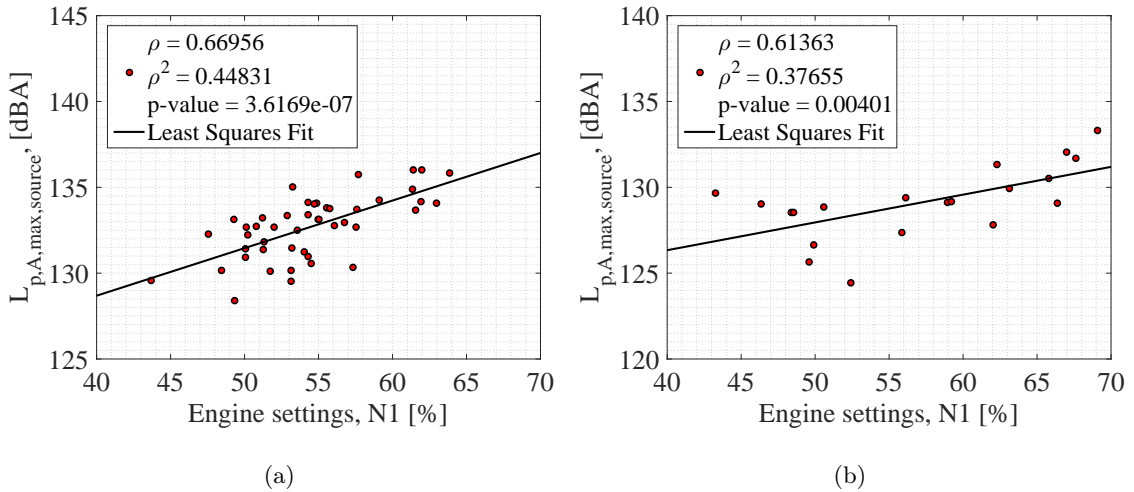


Fig. 6: Correlation analysis results (without beamforming) between the  $L_{p,A,max}$  and the engine fan settings for: (a) the Boeing 737 (series 700, 800 and 900) and (b) the Fokker 70.

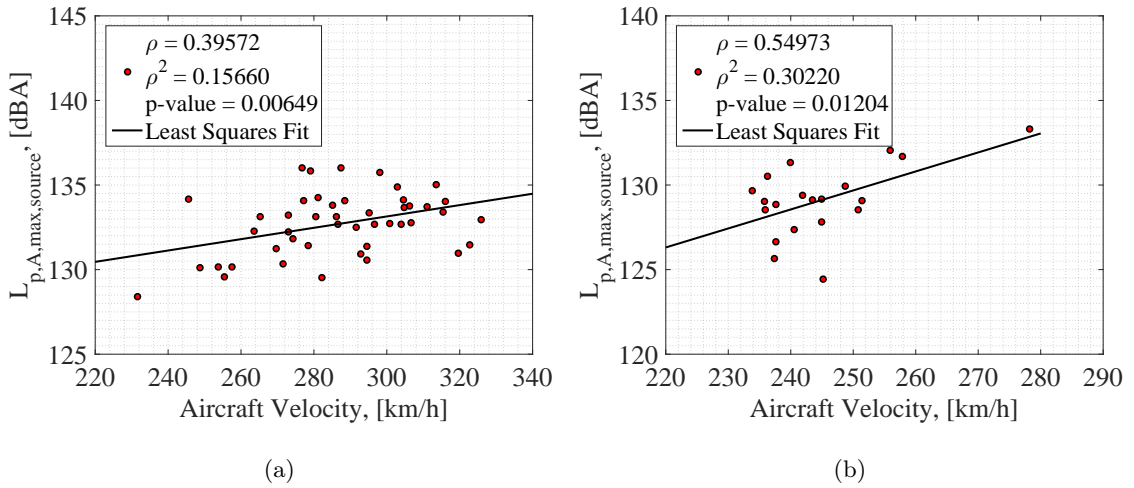


Fig. 7: Correlation analysis results (without beamforming) between the  $L_{p,A,max}$  and the aircraft velocity for: (a) the Boeing 737 (series 700, 800 and 900) and (b) the Fokker 70.

However, since N1% and the aircraft speed are also correlated ( $\rho \approx 0.80$ ), conclusions about the exact contribution of these parameters to the variability cannot be drawn. Therefore, in the next subsection, beamforming will be applied. This allows for investigating the noise from the different aircraft components separately. In this paper, the focus is placed on the noise from the engines, which is expected to be influenced by the engine settings, and the noise from the airframe, which is expected to be determined by the aircraft speed.

## B. Assessment of noise level variations using beamforming

### 1. Engine noise

For studying the variation of the noise levels at an aircraft component level, a correlation analysis was also performed after applying functional beamforming to the acoustic data. This subsubsection focuses on the sound generated by the engines. The times selected for this analysis span from 0.2 s before the time overhead to 0.1 s before the time overhead. Figure 8 contains one representative example of beamforming source plots for both aircraft types. These plots were obtained from the incoherent summation of the beamform source plots at the individual frequencies over the full band of available frequencies (from 50 to 11,200 Hz) using a 10 Hz frequency step. Also, indicated in the plots as black rectangles are the location of the engines. It can be clearly observed that the engines are the dominant noise source for the Boeing 737-800 case. For the Fokker 70 this is less clear.

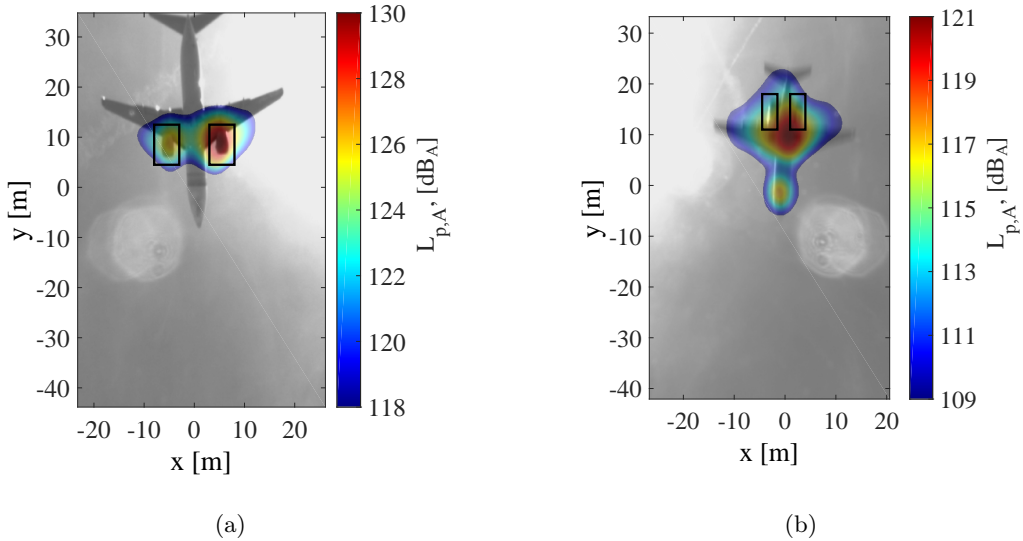


Fig. 8: Beamforming source plots for a frequency range from 50 to 11,200 Hz using functional beamforming with  $\nu = 100$  of (a) A Boeing 737-800 flyover. (b) A Fokker 70 flyover. The black rectangles show the areas of study for the variability analysis. The time interval spans from 0.2 to 0.1 s before the time overhead.

Figure 9 shows the overall  $L_{p,A}$  measured in the selected area (black rectangles of Fig. 8) plotted versus the engine setting. In addition to the overall  $L_{p,A}$  values, the  $L_{p,A}$  values obtained

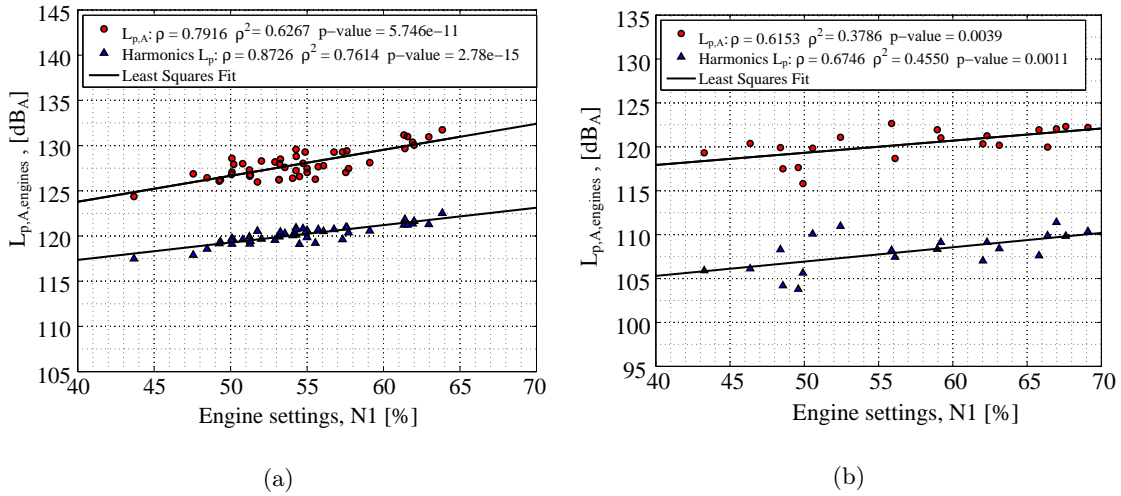


Fig. 9: Correlation analysis results after applying functional beamforming and considering the engines overall  $L_{p,A}$  and engine harmonics  $L_{p,A}$  with respect to the engine fan settings for (a) the Boeing 737 (series 700, 800 and 900) case and (b) the Fokker 70 case.

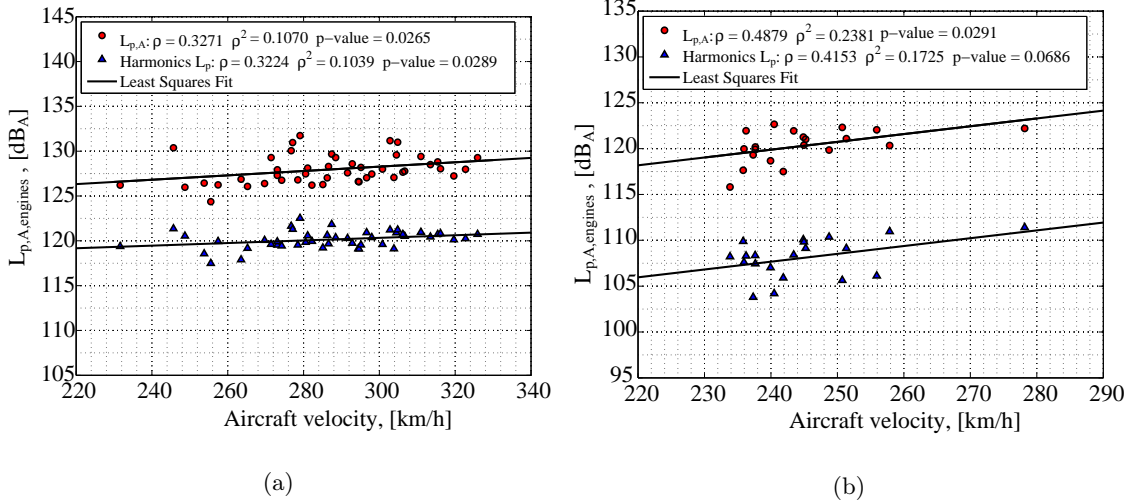


Fig. 10: Correlation analysis results after applying functional beamforming and considering the engines overall  $L_{p,A}$  and engine harmonics  $L_{p,A}$  with respect to the aircraft velocity for (a) the Boeing 737 (series 700, 800 and 900) case and (b) the Fokker 70 case.

from the incoherent summation of the source plots for only the frequencies around the BPF and its harmonics are also shown. Especially for this latter case, the increase in the correlation coefficients with respect to the engine fan settings compared to the case without applying beamforming is substantial, explaining more than 75% of the observed total variation of the  $L_{p,A}$  at the engines

for the BPF harmonics frequencies in the Boeing 737 case. This can be explained because the contributions from other noise sources are largely eliminated, due to the selection of an appropriate spatial area and frequencies. A comparable study by Simons et al. [10] showed similar results. For the Fokker 70 lower correlations are found.

On the other hand, the correlation of the noise levels with the aircraft velocity (see Fig. 10) is now lower than for the case without beamforming, even being non-significant for the Fokker 70 engine BPF harmonics case ( $p$ -value  $> 0.05$ ). This is because an increase in aircraft velocity is expected to mostly increase the airframe noise [40–42], and because the main contributors of the airframe noise are the landing gear system and the high-lift devices, engine noise is affected to a lesser extent by aircraft velocity. With this reasoning in mind, the larger correlation of the overall  $L_{p,A}$  of the Fokker 70 with the aircraft velocity shown in Fig. 7 (b) can be explained, because airframe noise is expected to be more significant for this aircraft type. This is further investigated in the following subsubsection.

## 2. Airframe noise

After observing the relatively large correlation of the  $L_{p,A,max}$  with the aircraft velocity for the Fokker 70 and the fact that airframe noise is dominant in the beamforming source plots (see Fig. 8 (b)), it was decided to perform an additional correlation study between the noise coming from the landing gear system and the aircraft velocity for this aircraft type. A distinction between the sound signals emitted at the nose landing gear and the main landing gear was made, as seen in the two considered areas in Fig. 11 (a). The selected conditions are the same as for the engine noise case: a time interval from 0.2 to 0.1 s before the time overhead.

Figure 11 (b) presents the overall  $L_{p,A}$  of the two sources with respect to the aircraft velocity. The linear least-squares fit is included for each source, as well as the sixth power law with the aircraft velocity, commonly used for compact sources, such as the landing gear [40–43]. It can be seen that the three lines approximately have the same slope. A significantly higher correlation coefficient (0.83) is obtained for the airframe noise case compared to the ones for the engine noise dependency with the fan rotational speed (0.67 and 0.62, see Figure 9 (b)). These results highlight

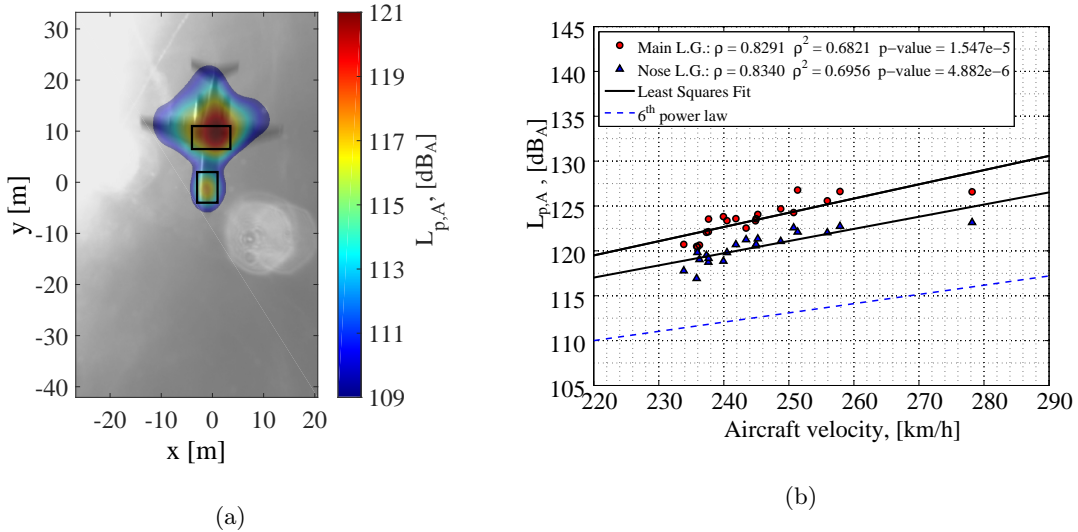


Fig. 11: (a) Beamforming source plot for a frequency range from 50 to 11,200 Hz using functional beamforming with  $\nu = 100$  of a Fokker 70 flyover. The black rectangles show the areas of study for the variability analysis. The time interval ranges from 0.2 to 0.1 s before the time overhead. (b) Correlation analysis for the Fokker 70 landing gear noise with respect to the aircraft velocity.

the importance of airframe noise and confirm its dependency with the source velocity. Other aircraft types, such as the Airbus A320, also presented dominant airframe noise sources [14, 36]. Due to the limited number of flyovers the A320 results are not presented in this paper.

Even if airframe noise is less dominant for the Boeing 737 “Next Generation” case, a similar correlation study was performed for the noise coming from the nose landing gear and the trailing edge devices (T.E.D.), with respect to the aircraft velocity. These two sources were selected because they were distinguishable in most flyover source plots, unlike the main landing gear, which was often masked by the engine noise. Unfortunately, there was no information available about the deflection angles of the T.E.D. for the flyovers in this research, but, during approach, one can expect similar values. The conditions for the beamforming analysis were kept constant. Figure 12 (a) illustrates an example of a Boeing 737-800 flyover with the selected areas for the analysis indicated as black boxes. The fifth power law with the air speed for non-compact objects [43, 44], such as the T.E.D., is also represented in Fig. 12 (b), because it seems to fit the T.E.D. noise behavior in a better way than the sixth power law. The correlation coefficient values obtained with the aircraft velocity

( $\rho \approx 0.80$ ) are similar to the ones obtained for the Fokker 70 landing gear system. However, the airframe contribution to the total noise is lower for the Boeing 737 “Next Generation” case.

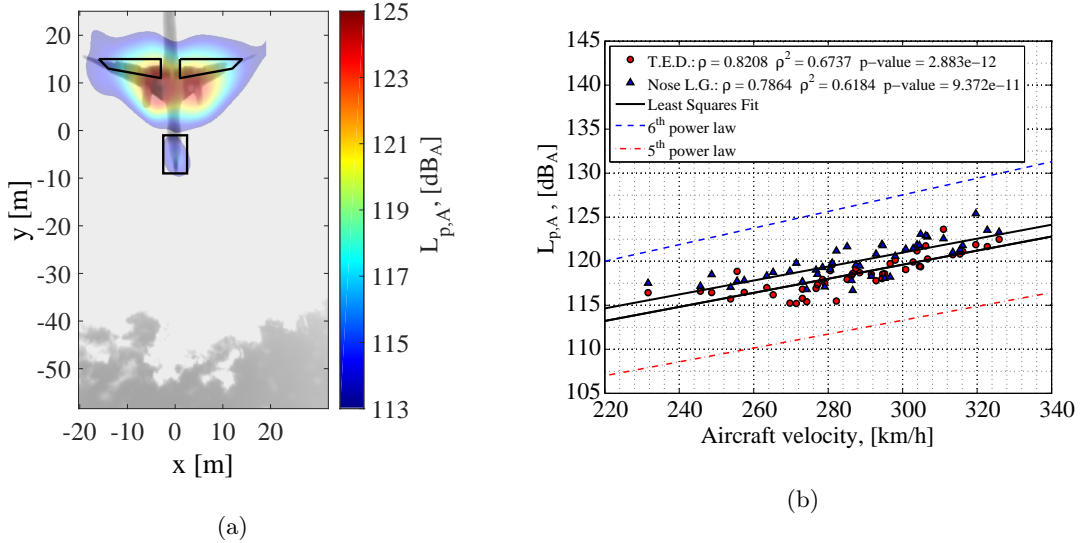


Fig. 12: (a) Beamforming source plot for a frequency range from 50 to 11,200 Hz using functional beamforming with  $\nu = 100$  of a Boeing 737-800 flyover. The black boxes show the areas of study for the variability analysis. The time interval ranges from 0.2 to 0.1 s before the time overhead. (b) Correlation analysis for the Boeing 737 noise from the nose landing gear and from the T.E.D. with respect to the aircraft velocity.

### 3. Relative contribution and variability of the aircraft noise sources

To visualize the relative contributions of the analyzed noise sources on the aircraft and their variability at the same time, the boxplots in Fig. 13 are presented for the Boeing 737 “Next Generation” and the Fokker 70, respectively.

In the first case (Fig. 13(a)), the engines are the main noise source, with an average overall  $L_{p,A}$  around 4 dB under the average total overall  $L_{p,A}$ . On the other hand the airframe noise sources studied (T.E.D. and the nose landing gear) present an average overall  $L_{p,A}$  approximately 12 dB lower than the total. The total overall  $L_{p,A}$  variability (6.9 dB) is comparable to that of the dominant noise source, i.e., the engine (7.4 dB). The variability of the T.E.D. and nose landing gear is slightly higher (8.4 dB and 8.7 dB, respectively). However, these have a limited contribution to

the total noise level.

For the Fokker 70 (Fig. 13(b)), it was shown that the main landing gear is the strongest noise source presenting an average overall  $L_{p,A}$  approximately 4 dB lower than the average total overall  $L_{p,A}$ . This time, the contribution of the engines is relatively lower, being approximately the same as the nose landing gear, whose average values are 8 dB lower than the total. The variability of the total overall  $L_{p,A}$  (7.5 dB) is now slightly larger than the overall  $L_{p,A}$  variabilities of the different sources: engines (6.8 dB), main landing gear (6.4 dB) and nose landing gear (6.2 dB). It can be observed that the variabilities for both aircraft types are of the same order of magnitude.

Apart from the considerably lower thrust provided, one of the reasons why the engine noise from the Fokker 70 is relatively less dominant than the one from the Boeing 737 “Next Generation” can be the engines location. Figure 14 presents one picture of each aircraft type during operating conditions [45, 46]. It can be observed that, whereas the engines of the Boeing 737 “Next Generation” are placed directly under the wing, the engines of the Fokker 70 are placed at the back of the fuselage over the wing, allowing for some noise shielding, especially for noise coming from the engine fan. In addition, the average BPF value of the Fokker 70 is higher than the one for the Boeing 737, and because higher frequencies are usually shielded more efficiently, this fact may explain as well why the tonal harmonic peaks from the fan were not very clear for the Fokker 70 in Fig. 5 (b).

## VI. Conclusions

In this paper the issue of noise variability for aircraft observed directly under the flight path was analyzed. Large sound pressure level variations for the same aircraft type are observed, hence posing a problem when assessing the noise levels around airports and when enforcing environmental laws. The noise assessment models usually employ Noise-Power-Distance tables, which do not consider these variations adequately and only provide fixed values of actual aircraft noise levels. In this research, the noise variability was assumed to depend mostly on the emitted noise at the source, i.e., the aircraft itself, neglecting the effects of a variable atmosphere.

Noise levels of 115 landing aircraft were recorded in a full scale field experiment using a 32 microphone phased array at Amsterdam Schiphol Airport. After correcting the data taking into account propagation effects, Doppler effect and background noise, the engine fan settings were

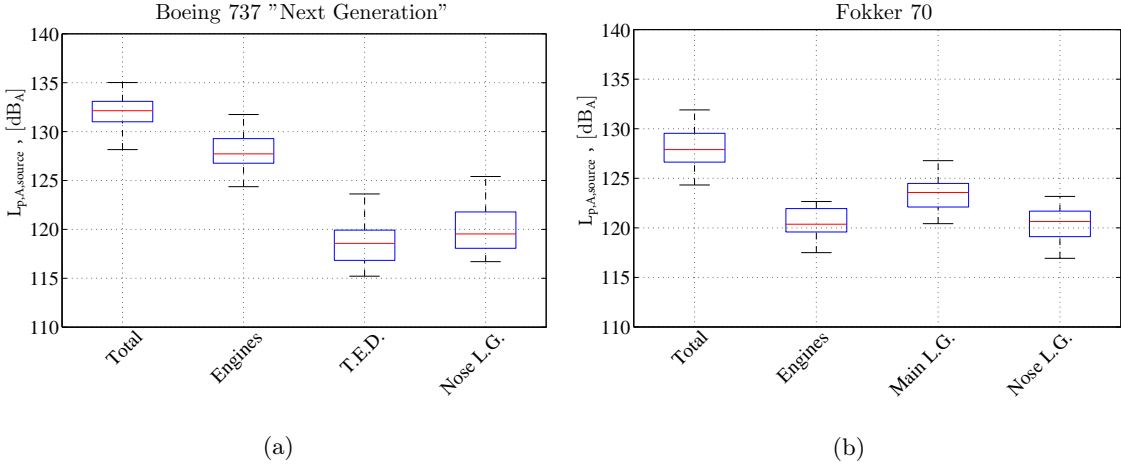


Fig. 13: Boxplot of the total overall  $L_{p,A}$  and the overall  $L_{p,A}$  at different aircraft components for  
 (a) the Boeing 737 “Next Generation” (b) the Fokker 70. On each box, the central mark is the  
 median, the edges of the box are the 25<sup>th</sup> and 75<sup>th</sup> percentiles and the whiskers extend to the most  
 extreme data points.



Fig. 14: (a) A Boeing 737-800 [45]. (b) A Fokker 70. [46]

determined by analyzing the typical harmonic tonal peaks from the fan noise in the spectrograms.

The  $L_{p,A,\max}$  variability observed directly under the flight path was approximately 7 dB for several landings of two aircraft types (Boeing 737 “Next Generation” and Fokker 70). A correlation analysis showed that the  $L_{p,A,\max}$  is highly related to the fan rotational speed of the turbofan engines. Correlation coefficients of around 0.67 are obtained for the variation of the  $L_{p,A,\max}$  with the engine settings, meaning that almost 45% of the total observed variation can be explained by changes in the engine fan settings. The correlation with the aircraft velocity had lower values, but

still explains more than 16% of the total variation observed.

The microphone array provides beamforming source plots which give information about the location and strength of the noise sources on the aircraft. After applying a beamforming technique called functional beamforming to the acoustic data and focusing only on the engines positions, it was found that the change in the engine fan settings can now explain more than 75% of the variation of the engine  $L_{p,A}$  for the Boeing 737 “Next Generation” and 45% for the Fokker 70. However, the correlation with the aircraft velocity is considerably lower this time, because it does not affect the engine noise in a considerable way. A similar analysis applied to the landing gear system of the Fokker 70 and the nose landing gear and T.E.D. of the Boeing 737, determined that differences in the aircraft velocity explain almost 70% of the noise level changes of these sources. In general, the remaining unexplained percentages of variability could be attributed to the sound source directivity, because the relative positions of each aircraft with respect to the array were not exactly the same.

In conclusion, to partly solve the issue of airport noise assessment due to the large noise level variations for the same aircraft type, it is highly recommended to include more accurate aircraft engine fan setting data into the models for noise contour calculations around airports. Moreover, airframe noise has proven to be the dominant source for some aircraft types, such as the Fokker 70 or the Airbus A320. Its dependency with the aircraft velocity has been confirmed.

Moreover, additional research is recommended for future work, such as the consideration of different sound metrics and, of course, the extension of this study to a larger number of aircraft types and flyover number. Studying the sound radiation directivity pattern is also a topic to be investigated, especially if a larger microphone array is employed.

## References

- [1] Hansell, A., Blangiardo, M., Fortunato, L., Floud, S., de, H. K., Fecht, D., Ghosh, R., Laszlo, H., Pearson, C., Beale, L., Beevers, S., Gulliver, J., Best, N., Richardson, S., and Elliott, P., “Aircraft noise and cardiovascular disease near Heathrow airport in London: small area study,” *British Medical Journal*, Vol. 347, 2013.
- [2] “Current Market Outlook 2013-2032,” Tech. rep., Boeing Commercial Airplanes, USA., 2013.
- [3] “Procedure for the Calculation of Airplane Noise in the Vicinity of Airports, Aerospace Information

Report AIR 1845," Tech. rep., Society of Automotive Engineers, Inc. (SAE) - Committe on Aircraft Noise (SAE A-21), 400 Commonwealth Drive, Warrendale, PA 15096, January 1986.

- [4] "Recommended method for computing noise contours around airports (ICAO Circular 205-AN/1/25)," Tech. rep., International Civil Aviation Organization (ICAO), Montreal, Canada., 1988.
- [5] "CEAC Doc. 29. Report on Standard method of Computing Noise Contours around Civil Airports. Volumes 1&2," Tech. rep., European Civil Aviation Conference (ECAC), 2005, 3<sup>rd</sup> edition.
- [6] He, B., Dinges, E., Hemann, J., Rickel, D., Mirsky, L., Roof, C., Boeker, E., Gerbi, P., and Senzig, D., "Integrated Noise Model (INM) Version 7.0 User's Guide," Tech. rep., Federal Aviation Administration (FAA) - U.S. Department of Transportation, Washington, DC, April 2007, Report No. FAA-AEE-07-04.
- [7] Boeker, E., Dinges, E., He, B., Fleming, G., Roof, C., Gerbi, P., Rapoza, A., and Hemann, J., "Integrated Noise Model (INM) Version 7.0 User's Guide," Tech. rep., Federal Aviation Administration (FAA) - U.S. Department of Transportation, Washington, DC, April 2008, Report No. FAA-AEE-08-01.
- [8] Bergmans, D., Arntzen, M., and Lammen, W., "Noise attenuation directly under the flight path," Tech. Rep. NLR-TP-2011-262, National Aerospace Laboratory (NLR), Anthony Fokkerweg 2, 1059 CM Amsterdam, P.O. Box 90502, 1006 BM Amsterdam, The Netherlands, November 2011.
- [9] Hebly, S., Sindhamani, V., Arntzen, M., Bergmans, B., and Simons, D., "Noise attenuation directly under the flight path in varying atmospheric conditions," Tech. Rep. NLR-TP-2013-453, National Aerospace Laboratory (NLR), Anthony Fokkerweg 2, 1059 CM Amsterdam, P.O. Box 90502, 1006 BM Amsterdam, The Netherlands, 2013.
- [10] Simons, D. G., Snellen, M., Midden, B., Arntzen, M., and Bergmans, D. H. T., "Assessment of noise level variations of aircraft fly-overs using acoustic arrays," *Journal of Aircraft*, Vol. 52, No. 5, September-October 2015, pp. 1625–1633.
- [11] Dougherty, R. P., "Functional Beamforming," *5<sup>th</sup> Berlin Beamforming Conference, February 19-20 2014, Berlin, Germany.*, GFaI, e.V., Berlin, February 2014.
- [12] Dougherty, R. P., "Functional Beamforming for Aeroacoustic Source Distributions," *20<sup>th</sup> AIAA/CEAS Aeroacoustics Conference. June 16-20 2014. Atlanta GA, USA.*, 2014, AIAA paper 2014-3066.
- [13] Mueller, T., *Aeroacoustic Measurements*, Springer Science & Business Media, 2002, ISBN-978-3-642-07514-8.
- [14] Merino-Martinez, R., Snellen, M., and Simons, D. G., "Functional beamforming applied to imaging of flyover noise on landing aircraft," *Journal of Aircraft*, Vol. 53, No. 6, November-December 2016, pp. 1830–1843.
- [15] van der Goot, R., Hendriks, J., Schepers, K. Y. W., Hermans, G. and van der Wal, W., and Simons,

- D. G., "A low cost, high resolution acoustic camera with a flexible microphone configuration," *4<sup>th</sup> Berlin Beamforming Conference, February 22-23 2012, Berlin, Germany*, GFaI, e.V., Berlin, February 2012.
- [16] Royal Netherlands Meteorological Institute (KNMI) website, "<http://www.knmi.nl/klimatologie/uurgegevens/>," Accessed in August 2013.
- [17] European Aviation Safety Agency (EASA) website, "<http://www.easa.europa.eu>," Accessed in August 2013.
- [18] Howell, G. P., Bradley, M. A., McCormick, M. A., and Brown, J. D., "De-Dopplerization and acoustic imaging of aircraft flyover noise measurements," *Journal of Sound and Vibration*, Vol. 105, No. 1, Feb 1986, pp. 151–167.
- [19] Arntzen, M., *Aircraft noise calculation and synthesis in a non-standard atmosphere*, Ph.D. thesis, Delft University of Technology, 2014.
- [20] Ruijgrok, G., *Elements of aviation acoustics*, VSSD, Second ed., 2007, ISBN 1090-6562-155-5.
- [21] Johnson, D. H. and Dudgeon, D. E., *Array Signal Processing, Concepts and Techniques*, P T R Prentice Hall, Englewood Cliffs, 1993, ISBN: 9780130485137.
- [22] van Veen, B. D. and Buckley, K. M., "Beamforming: A Versatile Approach to Spatial Filtering," *IEEE ASSP Magazine*, Vol. 5, No. 2, April 1988, pp. 4–24.
- [23] Sijtsma, P., "Phased array beamforming applied to wind tunnel and fly-over tests," Tech. Rep. NLR-TP-2010-549, National Aerospace Laboratory (NLR), Anthony Fokkerweg 2, 1059 CM Amsterdam, P.O. Box 90502, 1006 BM Amsterdam, The Netherlands, December 2010.
- [24] Liu, Y., Quayle, A. R., Dowling, A. P., and Sijtsma, P., "Beamforming correction for dipole measurement using two-dimensional microphone arrays," *Journal of the Acoustical Society of America*, Vol. 124, No. 1, July 2008, pp. 182–191.
- [25] Camier, C., Padois, T., Provencher, J., Gauthier, P., Berry, A., Blais, J., Patenaude-Dufour, M., and Lapointe, R., "Fly-over source localization on civil aircraft," *19<sup>th</sup> AIAA/CEAS Aeroacoustics Conference. May 27-29 2013. Berlin, Germany*, 2013, AIAA paper 2013-2261.
- [26] Dougherty, R. P., Ramachandran, R. C., and Raman, G., "Deconvolution of Sources in Aeroacoustic Images from Phased Microphone Arrays Using Linear Programming," *19<sup>th</sup> AIAA/CEAS Aeroacoustics Conference, May 27-29 2013, Berlin, Germany*, May 2013, AIAA paper 2013-2210.
- [27] Herold, G. and Sarradj, E., "Preliminary Benchmarking of Microphone Array Methods," *5<sup>th</sup> Berlin Beamforming Conference, 19-20 February 2014, Berlin, Germany*, GFaI, e.V., Berlin, February 2014.
- [28] Ishii, Y., Hald, J., Ishii, T., Oinuma, H., Nagai, K., Yokokawa, Y., and Yamamoto, K., "High-Resolution Fly-Over Beamforming Using a Practical Array," *5<sup>th</sup> Berlin Beamforming Conference, February 19-20*

2014, Berlin, Germany, GFaI, e.V., Berlin, February 2014.

- [29] Sijtsma, P. and Stoker, R., "Determination of Absolute Contributions of Aircraft Noise Components Using Fly-over Array Measurements," *10<sup>th</sup> AIAA/CEAS Aeroacoustics Conference, May 10-12 2004, Manchester, United Kingdom*, 2004, AIAA paper 2004-2958.
- [30] Sijtsma, P. and van der Wal, H., "Identification of noise sources on civil aircraft in approach using a phased array of mmicrophone," Tech. Rep. NLR-TP-2004-166, National Aerospace Laboratory (NLR), Anthony Fokkerweg 2, 1059 CM Amsterdam, P.O. Box 90502, 1006 BM Amsterdam, The Netherlands, April 2004.
- [31] Michel, U., Barsikow, B., Helbig, J., Hellmig, M., and Schüttelzel, M., "Flyover noise measurements on landing aircraft with a microphone array," *4<sup>th</sup> AIAA/CEAS Aeroacoustics Conference, June 2-4 1998, Toulouse, France*, June 1998, AIAA paper 1998-2336.
- [32] Sijtsma, P., "Experimental techniques for identification and characterisation of noise sources," Tech. Rep. NLR-TP-2004-165, National Aerospace Laboratory (NLR), Anthony Fokkerweg 2, 1059 CM Amsterdam, P.O. Box 90502, 1006 BM Amsterdam, The Netherlands, April 2004.
- [33] Sarradj, E., "Three-Dimensional Acoustic Source Mapping with Different Beamforming Steering Vector Formulations," *Advances in Acoustics and Vibration*, Vol. 2012, 2012, pp. 1–12.
- [34] Lord Rayleigh, F. R. S., "XXXI. Investigations in Optics with special reference to the Spectroscope," *The London, Edinburgh and Dublin Philosophical Magazine and Journal of Science*, Vol. 8, No. 49, October 1879, pp. 261–274.
- [35] Merino-Martinez, R., Snellen, M., and Simons, D. G., "Functional Beamforming Applied to Full Scale Landing Aircraft," *6<sup>th</sup> Berlin Beamforming Conference, February 29– March 1 2016, Berlin, Germany*., 2016.
- [36] Merino-Martinez, R., Bertsch, L., Snellen, M., and Simons, D. G., "Analysis of landing gear noise during approach," *22<sup>nd</sup> AIAA/CEAS Aeroacoustics Conference. May 30 - June 1 2016. Lyon, France*., 2016, AIAA paper 2016-2769.
- [37] Merino-Martinez, R., Snellen, M., and Simons, D. G., "Determination of Aircraft Noise Variability Using an Acoustic Camera," *23<sup>rd</sup> International Congress on Sound and Vibration, July 10-14 2016, Athens, Greece*., 2016.
- [38] Arntzen, M. and Simons, D. G., "Modeling and synthesis of aircraft flyover noise," *Journal of Applied Acoustics*, Vol. 84, No. 5, 2014, pp. 99–106.
- [39] Snellen, M., Merino-Martinez, R., and Simons, D. G., "Assessment of aircraft noise sources variability using an acoustic camera," *5<sup>th</sup> CEAS Air & Space Conference. Challenges in European Aerospace*.

*September 7-11 2015, Delft, Netherlands, 2015.*

- [40] Dobrzynski, W. and Buchholz, H., "Full-scale noise testing on Airbus landing gears in the German Dutch Wind Tunnel," *3<sup>rd</sup> AIAA/CEAS Aeroacoustics Conference. May 12-14 1997. Atlanta GA, USA.*, 1997, AIAA paper 1997-1597.
- [41] Fink, M., "Noise component method for airframe noise," *4<sup>th</sup> AIAA Aeroacoustics Conference. October 3-5 1977, Atlanta, Georgia, USA.*, 1977, AIAA Paper 1977-1271.
- [42] Curle, N., "The influence of solid boundaries upon aerodynamic sound," *Proceedings of Royal Society of London A*, Vol. 231, No. 1187, September 1955, pp. 505–514.
- [43] Delfs, J., *Basics of Aeroacoustics - Lecture notes at Technische Universität Braunschweig*, VSSD, 2011.
- [44] Ffowcs Williams, J. and Hall, L., "Aerodynamic sound generation by turbulent flow in the vicinity of a scattering half plane," *Journal of Fluid Mechanics*, Vol. 40, No. 4, 1970, pp. 657–670.
- [45] Source for Boeing 737-800 picture, "<http://www.boeing.com/commercial/737ng/>," Accessed in January 2016.
- [46] Source for Fokker 70 picture, "<https://commons.wikimedia.org>," Accessed in January 2016.